Catal Lett (2008) 123:282–288
DOI 10.1007/s10562-008-9420-x

Effects of Cocatalyst and Calcination Temperature on Photocatalytic Hydrogen Evolution Over $BaTi_4O_9$ Powder Synthesized by the Polymerized Complex Method

Wei Sun · Shuqing Zhang · Cheng Wang · Zhixiang Liu · Zongqing Mao

Received: 18 December 2007 / Accepted: 23 January 2008 / Published online: 12 February 2008

Abstract $BaTi_4O_9$ powders with improved crystal perfection and relatively large surface area were synthesized by the polymerized complex (PC) method calcined at reduced temperatures (700–1,000 °C) relative to the solid-state reaction (SSR) method. $BaTi_4O_9$ with a unique pentagonal-prism tunnel structure, combined with different cocatalysts (Pt, Ru, Ni, Cu, Co) as promoters, was investigated towards photocatalytic reactions for H_2 evolution from pure water and aqueous ethanol solution. $Pt/BaTi_4O_9$ achieved the highest activity from ethanol solution, and subsequently it was focused to study the effect of calcination temperature on photocatalytic activities. The maximum quantum yield for H_2 evolution from pure water and ethanol solution was obtained at 700 and 800 °C separately, with the value of 0.9% and 11.7% over $Pt/BaTi_4O_9$ photocatalysts.

Keywords $BaTi_4O_9$ · Polymerized complex method · Photocatalytic activity · Hydrogen evolution

1 Introduction

TiO_2-based compounds have been extensively investigated as efficient photocatalysts for photodecomposition of water under UV irradiations [1–5]. The compounds of barium titanates are of great importance in materials science due to their attractive ferroelectric and dielectric properties. Special interests have been paid to the photocatalytic applications of these materials with a TiO_2-rich content, such as $BaTi_4O_9$ [6–8], $BaTi_5O_{11}$ [9], $Ba_4Ti_{13}O_{30}$ [10] and etc. $BaTi_4O_9$ combined with RuO_2 has emerged as a new class of potential photocatalyst for photocatalytic water decomposition [6]. The high photocatalytic performance over RuO_2–$BaTi_4O_9$ is mainly ascribed to the unique pentagonal–prism tunnel structure of $BaTi_4O_9$. In the orthorhombic structure of $BaTi_4O_9$ as shown in Fig. 1, the edge- and corner-sharing of TiO_6 octahedra give rise to the chemical twin tunnels which accommodate the Ba atoms in a pentagonal prismatic coordination [11]. This unique structure has two distinctive advantages in photocatalytic reactions: (1) the dipole moment resulted from the heavily distorted TiO_6 octahedra are considered to be useful for electron-hole separation upon photoexcitation [12]; (2) the characteristic structure provides the form of a concave site with a ridge like a "nest", which likely makes a geometric barrier to prevent the loading cocatalyst from growing and aggregating [2]. Recently, the advantage of Pechini-type polymerized complex (PC) method to the traditional solid-state reaction (SSR) method has been greatly confirmed for the improved crystalline homogeneity and photocatalytic activity of the product [13, 14], which is especially meaningful for RuO_2–$BaTi_4O_9$ [7, 8], from the aspect that the suppressed growth of unstoichiometric impurities and highly dispersive RuO_2 particles can be achieved by the PC method.

In this article, some new insights have been brought forward in the investigation for different kinds of loading species to the photocatalytic H_2 evolution over $BaTi_4O_9$ photocatalyst from both pure water and aqueous ethanol solution. The predominant performances over $Pt/BaTi_4O_9$ towards the introduction of ethanol were first reported here, and the impact of calcination temperature on the photoactivity of $Pt/BaTi_4O_9$ was described in details.

W. Sun · C. Wang · Z. Liu · Z. Mao (✉)
Institute of Nuclear and New Energy Technology, Tsinghua University, Beijing 100084, P.R. China
e-mail: maozq@tsinghua.edu.cn

S. Zhang
College of Material Science and Chemistry Engineering, China University of Geosciences, Wuhan 430074, P.R. China

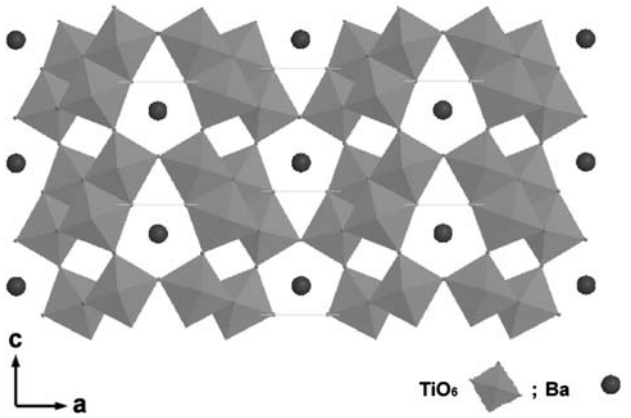

Fig. 1 A schematic representation of $BaTi_4O_9$ with a unique pentagonal–prism tunnel structure

2 Experimental

All chemicals were of analytical grade and used without further purification. Powders of $BaTi_4O_9$ were synthesized by the PC route according to the procedures in literatures [7, 8]. Here $Ba(CH_3COO)_2$ instead of $BaCO_3$ were selected as Ba sources for better solubility and improved interactions between Ba and Ti complexes. About 0.02 mol of TBOT was dissolved into 0.8 mol of ethylene glycol (EG), and subsequently 0.20 mol of citric acid (CA) was added to this solution. After complete dissolution of CA, an aqueous solution containing 0.05 mol of $Ba(Ac)_2$ was added and the mixture was magnetically stirred at ~50 °C for 2 h (pH = 5). The obtained transparent solution was then heated at 140–150 °C for several hours with continuous stirring to accelerate polyesterification between CA and EG, resulted in a highly viscous gel without any visible precipitation. The precursor of black powder was obtained by charring the gel at 350 °C for 2 h in an electric furnace. The product was finally synthesized by calcining the precursor in static air for 2 h at temperatures between 600 and 1,000 °C with an interval of 100 °C. For comparison, $BaTi_4O_9$ was also prepared by the conventional SSR method. A stoichiometric mixture of $BaCO_3$ and TiO_2 (P25, Degussa) was ground mechanically and then calcined at 1,100 °C for 10 h.

About 1.0 wt% Pt cocatalyst was loaded to obtain high activity from an aqueous $H_2PtCl_6 \cdot 6H_2O$ solution by a photodeposition method. For the comparative study between different loading species, 1.0 wt% MO_x (M = Ru, Ni, Cu, Co) was loaded by the impregnation method with an aqueous solution of $RuCl_3$, $Ni(NO_3)_2$, $Cu(NO_3)_2$ and $Co(NO_3)_2$, respectively. The impregnated $BaTi_4O_9$ was dried at 80 °C in water bath and then subjected to the reduction process in H_2 atmosphere at 500 °C for 2 h followed by oxidation in air at 200 °C for 1 h.

The crystal structures of synthesized powders were characterized by X-ray diffraction (XRD, D/Max-RB, Cu Kα). The surface area was determined by the Brunauer–Emmett–Teller method using nitrogen gas as absorbent (BET, NOVA 4000). The morphology of crystals was observed by transmission electron microscopy (TEM, JEOL JEM-1200EX). The diffuse reflectance UV-Vis absorption spectra were collected on a UV-Vis spectrometer (DRS, Hitachi U-3010). The photoluminescence emission spectra were recorded by a fluorescence spectrophotometer (PL, Perkin-Elmer LS55) with an excitation wavelength of 265 nm at room temperature.

Photocatalytic reactions for H_2 evolution were carried out in a gas-closed circulation system. The photocatalyst powder (0.1 g) was dispersed in deionized water (100 ml) or aqueous ethanol solution (100 ml of deionized water, 20 ml of C_2H_5OH) by means of magnetic stirring in a 390 ml reaction cell made of quartz glass. A 500 W high-pressure Hg lamp was used as the light source and irradiated from the top of the cell. To avoid the heating of the solution during illuminations, cool water was circulated through a quartz jacket around the wall of cell. The reaction temperature was constantly adjusted to 30 ± 2 °C. The amount of evolved H_2 was determined by gas chromatography (Shimazu GC-14B; TDX-01 column, TCD, Ar carrier) through a gas sampler (0.5 ml) which was directly connected to the reaction system.

The quantum yield is more meaningful than H_2 evolution rate to evaluate the performance of photocatalyst since the rate is normalized against the absorbed photons [15]. The apparent quantum yield was determined as below:

$$\text{Quantum yield} = [(2 \times \text{the amount of evolved } H_2)/ \text{the number of incident photons}] \times 100\%$$

The number of incident photons was calculated from the chemical actinometer of potassium ferrioxalate $[K_3Fe(C_2O_4)_3 \cdot 3H_2O]$, which was estimated to be 4.07×10^{-6} mol s^{-1}. In this case, it is considered that the 365 nm emission of the high-pressure Hg lamp is the major promoter of the reaction.

3 Results and Discussion

Figure 2 shows the XRD patterns of $BaTi_4O_9$ powders synthesized by the SSR method at 1,100 °C for 10 h and the PC method at 600–1,000 °C for 2 h. The PC-derived sample prepared at 600 °C was revealed as primarily amorphous solids. The crystallization was initiated after raising the calcination temperature to 700 °C, showing major phase of orthorhombic structure in good agreement with the diffraction pattern of $BaTi_4O_9$ (JCPDF 34-0070).

However, the presence of impurity phases including $BaTi_5O_{11}$, $BaTi_2O_5$, and $BaTiO_3$ were observed as well in PC-derived sample at 700 °C. When the calcination temperature was increased to 800–900 °C, the crystallinity of $BaTi_4O_9$ was greatly improved and phases of $BaTi_5O_{11}$ and $BaTiO_3$ completely disappeared from XRD patterns, leaving $BaTi_2O_5$ as a single impurity in bulk. For PC-derived sample at 1,000 °C, the crystal homogeneity was further improved whereas a new phase of $Ba_4Ti_{13}O_{30}$ substituted for $BaTi_2O_5$ as a tiny amount of impurity, indicating that even higher calcination temperature is required to obtain the absolute pure-phase of $BaTi_4O_9$. It has been reported in literature that the single-phase of $BaTi_4O_9$ can definitely be obtained by calcination at 1,100 °C with different CA contents by the PC method [16]. For the sample prepared by the SSR method at 1,100 °C for 10 h, it exhibited major $BaTi_4O_9$ phase with various impurity phases, such as $BaTi_2O_5$, $Ba_4Ti_{13}O_{30}$, $BaTiO_3$ and $BaTi_5O_{11}$. Moreover, a shift of the diffraction peak to higher angles ($\sim$0.15°) relative to standard position was observed over the SSR sample. As a consequence, it can be concluded that the PC method has the advantage in the improved homogeneity and accuracy of crystal growth of $BaTi_4O_9$ compound compared to the traditional SSR method.

Figure 3 shows the TEM images of all the $BaTi_4O_9$ samples. The particles of PC-derived powder at 600 °C exhibited relatively uniform morphology with average size of approximately 12 nm. It is evident that the nanoparticles

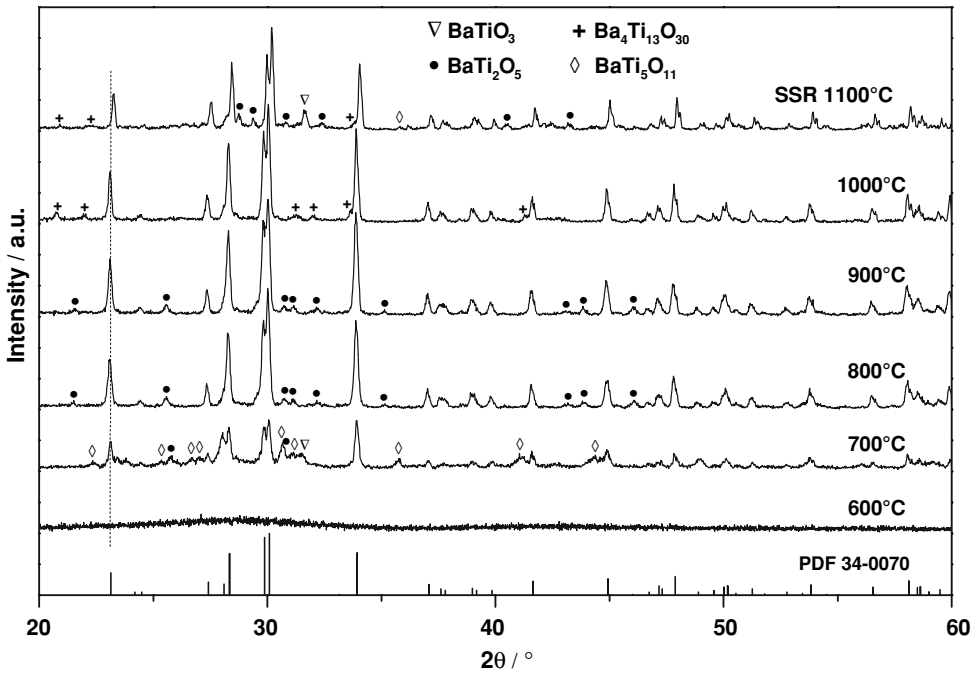

Fig. 2 XRD patterns of $BaTi_4O_9$ prepared by the PC method at different temperatures for 2 h and by the SSR method at 1,100 °C for 10 h

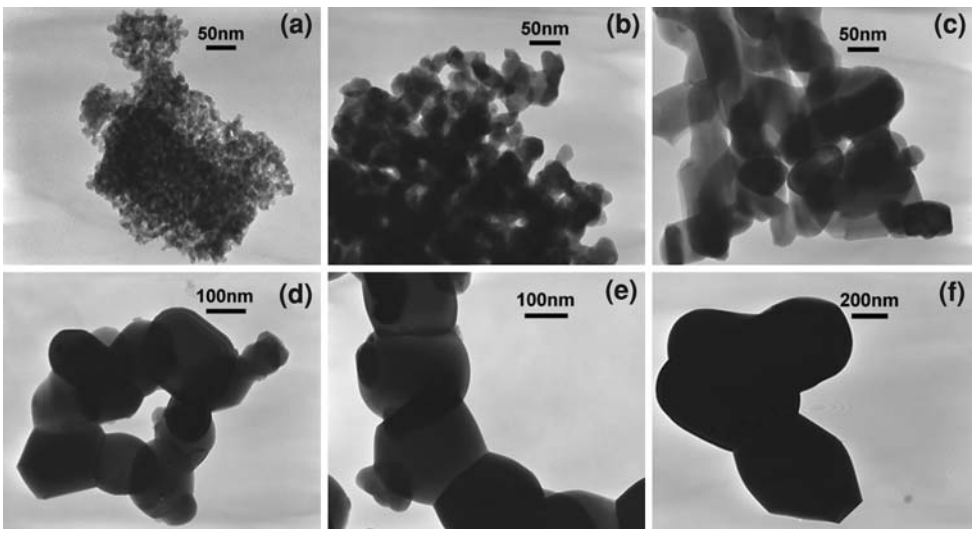

Fig. 3 TEM images of $BaTi_4O_9$ prepared by the PC method calcined at (**a**) 600 °C, (**b**) 700 °C, (**c**) 800 °C, (**d**) 900 °C, (**e**) 1,000 °C for 2 h and by the SSR method calcined at (**f**) 1,100 °C for 10 h

Table 1 Summaries of physical properties evaluated from XRD patterns, BET method and DRS of the $BaTi_4O_9$ powders

Calcination temperature (°C)	Synthesis	Impurities	Surface area ($m^2\ g^{-1}$)	Eg_a (eV)[a]	Eg_b (eV)[a]	λ_b (nm)
600	PC	Amorphous	28.43	3.32	2.88	348
700	PC	$BaTi_5O_{11}$, $BaTi_2O_5$, $BaTiO_3$	13.37	3.43	3.35	349
800	PC	$BaTi_2O_5$	6.22	3.55	3.46	347
900	PC	$BaTi_2O_5$	4.29	3.55	3.47	346
1000	PC	$Ba_4Ti_{13}O_{30}$	2.16	3.60	3.51	345
1100	SSR	$BaTi_2O_5$, $Ba_4Ti_{13}O_{30}$, $BaTiO_3$, $BaTi_5O_{11}$	1.07	3.61	3.47	344

[a] Caculated from the straight regions of the absorption coefficient $(\alpha h\nu)^2$ versus hν near the band edge: Eg_a is referred to the main obsorption edge and Eg_b is related with the slight absorption peak around λ_b

grow up with increasing calcination temperatures from 700 to 800 °C, and porous networks can be observed as well due to the burnout of organics during charring. The particle size increases markedly to 0.1–0.3 μm after raising temperatures to 1,000 °C, displaying highly dense particles with round corners. For the SSR sample calcined at 1,100 °C, dark images of large powders with higher electron density were observed, representing serious agglomeration of particles. The BET surfaces of these samples are summarized in Table 1. It is easy to understand that the surface area of PC-derived $BaTi_4O_9$ samples sharply decreases with increasing calcination temperatures, associated with the continuous crystal growth as shown in Fig. 3. Another important characteristic is that PC-derived samples possess relatively large surface areas compared to the SSR product. It is known that having a crystalline material with a large surface area is of practical importance for certain applications, particularly a catalytic application [13]. Thus it is anticipated that the PC-derived $BaTi_4O_9$ photocatalyst with improved crystal homogeneity and high surface area would exhibit higher catalytic activities than the SSR sample.

The diffuse reflection spectra of $BaTi_4O_9$ prepared by the SSR method and PC method at different temperatures are shown in Fig. 4a. The value of the band gaps for all samples were shown in Table 1, which was determined from the energy intercept by extrapolations of the straight regions of the absorption coefficient $(\alpha h\nu)^2$ versus hν for a direct allowed transition [17]. For the SSR sample, a shoulder peak at a wavelength of about 390 nm is presumably associated with the imperfect crystallization as revealed by XRD. An extended tail at the absorbance edge is observed for PC-derived sample at 600 °C, which can be probably related to the delocalized electronic levels in the forbidden gap introduced by amorphous clusters [18]. In addition, the PC-derived sample at 700 °C exhibits relatively higher absorption in the visible range, which could also be an evidence for the absorption of impurities. An interesting phenomenon can be detected that all the spectra display a slight absorption peak within the major absorption edge, which is signed as λ_b and listed in

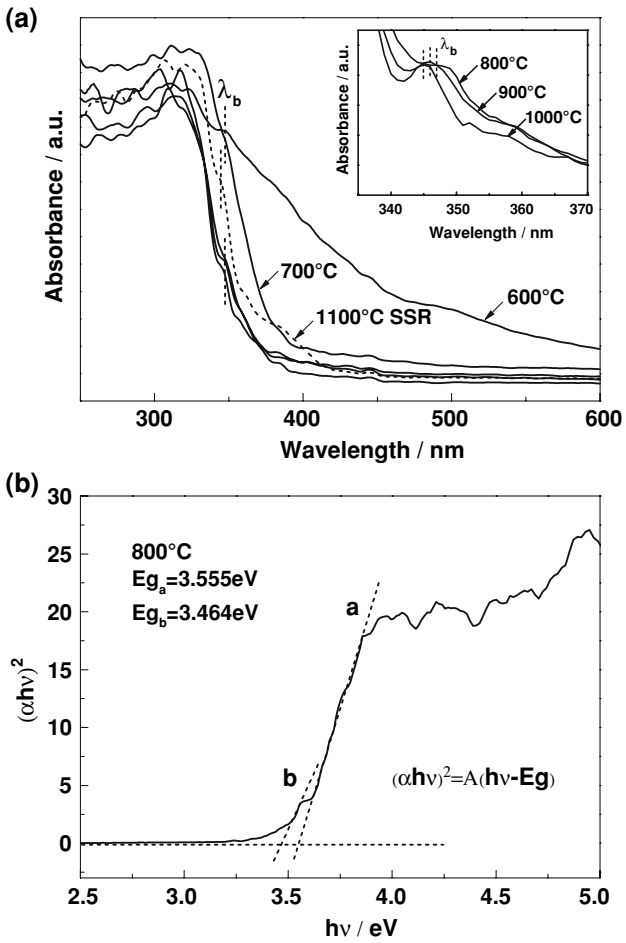

Fig. 4 (**a**) Diffuse reflectance spectra of $BaTi_4O_9$ prepared by the SSR method at 1,100 °C for 10 h and the PC method at different temperatures for 2 h, (**b**) The illustration for the determination of energy gap calculated by the extrapolations of the straight regions of the absorption coefficient $(\alpha h\nu)^2$ versus hν near the band edge over PC-derived $BaTi_4O_9$ prepared at 800 °C

Table 1. Apparently there will be two different values of the band gap obtained from the two slopes within the straight regions as illustrated in Fig. 4b. The band gap of Eg_b related to the slight peak is probably derived from the

absorption of impurity phases. For example, approximately the same value of Eg_b is obtained for PC-derived samples at 800 and 900 °C, which may result from the absorption of $BaTi_2O_5$ as the same major impurity for both samples. The band gap of Eg_a for $BaTi_4O_9$ (~3.55 eV) appears to slightly increase with increasing calcination temperatures, assumed to be due to the improved crystallinity of $BaTi_4O_9$ synthesized at increased temperatures.

The photoluminescence emission spectra have been widely used to investigate the efficiency of charge carrier trapping, immigration and transfer, and to understand the fate of electron/hole pairs in semiconductor particles [19]. Figure 5 shows the PL emission spectra with an excitation wavelength of 265 nm at room temperature. All the PC-derived $BaTi_4O_9$ prepared from 700 to 1,000 °C exhibit in approximately the same shape. The main emission peak at about 402 nm was attributed to a direct recombination of a conduction electron in Ti 3*d* orbital and a hole in O 2*p* valence band. The difference between the bandgap energy (~3.55 eV) and the emission peak energy (~3.08 eV), which is around 0.47 eV, is described as the Stokes shift due to the Frank–Condon effect [20]. The second highest emission peak at about 420 nm can be referred to the radiative recombination of excitons from impurities of unstoichiometric barium titanates. For SSR sample, it is evident that the main emission peak is transferred to around 420 nm, which indicates the recombination of excitons trapped by impurities becomes the major part of PL emission. In addition, impurities in bulk can enhance non-radiative recombination of the excited electrons [20], leading to the decrease in emission intensity of SSR sample. It appears that the PL intensity of PC-derived $BaTi_4O_9$ increases with increasing calcination temperature from 600 to 900 °C, which can be mainly attributed to the improved crystal integrity. The flat PL curve with low intensity of amorphous powder prepared at 600 °C can confirm the correlation between PL spectra and crystalline perfection. The occurred reduction in PL intensity of PC-derived sample at 1,000 °C may result from the decreased number of self-trapped excitons caused by enlarged particle size [21]. Besides this, the enhanced PL intensity for PC-derived sample at 800 and 900 °C may also be ascribed to the increased content of Ti^{3+} *d*-orbital surface states stabilized by oxygen vacancy in the forbidden gap [22], which is beneficial to retard the recombination of photogenerated electron-hole pairs in photocatalytic reactions.

Figure 6 shows the effect of different cocatalysts (Pt, Ru, Ni, Cu, Co), combined with PC-derived $BaTi_4O_9$ calcined at 900 °C, on the photocatalytic activity for H_2 evolution. As to the photoreaction of water splitting, a steady evolution of approximately stoichiometric amount of H_2 and O_2 was detected over NiO_x and RuO_x loaded $BaTi_4O_9$, and NiO_x is found to be the most effective promoter for $BaTi_4O_9$ in photocatalytic water splitting with an average H_2 evolution rate of 60 μmol h^{-1}. However, the formation of O_2 cannot be steadily observed on Pt, CuO_x and CoO_x loaded photocatalysts, among which CoO_x/$BaTi_4O_9$ can barely produce hydrogen either. In these cases, photogenerated holes in photocatalyst would generate ·OH radicals and O_2 molecules physisorbed or chemisorbed on the surface [23], which may progressively saturate the cocatalyst's surface, rendering it inactive for H_2 evolution after long periods [24] as shown from the inset. In order to facilitate the oxidation part of photoreaction, an additional 20 ml of ethanol was applied

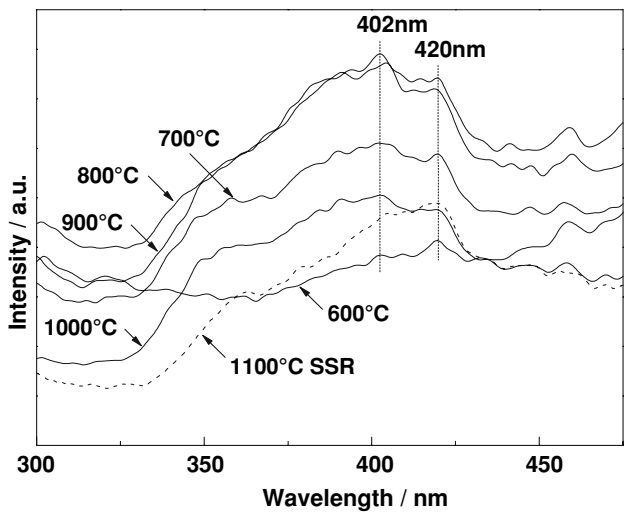

Fig. 5 Room-temperature PL spectra (λ_{ex} = 265 nm) of $BaTi_4O_9$ by the PC method at different temperatures for 2 h and by the SSR method at 1,100 °C for 10 h

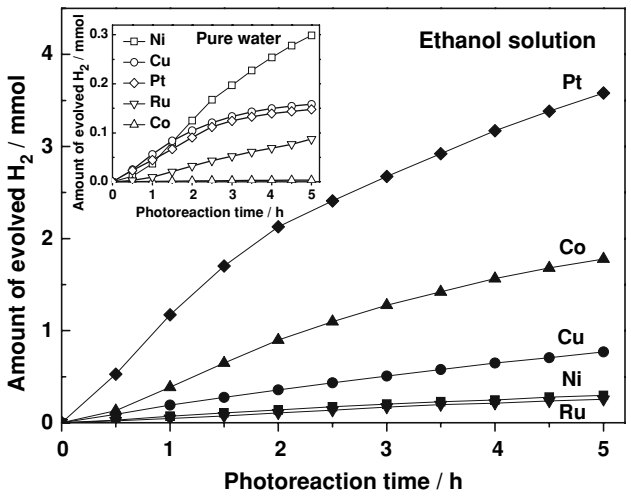

Fig. 6 Time courses of H_2 evolution from pure water (inset) and ethanol solution over $BaTi_4O_9$ support (900 °C PC) loaded with 1 wt% Pt by photodeposition method and 1 wt% MO_x (M = Ru, Ni, Cu, Co) treated after the reduction of impregnated $BaTi_4O_9$ at 500 °C for 2 h followed by oxidation at 200 °C for 1 h

as sacrificial reagent to obtain improved H_2 evolution. In contrast to the results from pure water, NiO_x and RuO_x performed low activity in aqueous ethanol solution compared to other cocatalysts, and the sacrificial reagent does not seem to make its contribution to promote photoreactions. However, the photocatalytic H_2 evolution over Pt, CoO_x and CuO_x loaded $BaTi_4O_9$ was greatly enhanced from ethanol solution. Pt/$BaTi_4O_9$ is testified as the most efficient photocatalyst with an average H_2 evolution rate of 716 μmol h^{-1}, implying that the loading of metallic Pt with high electric conductivity acts more efficient roles in trapping and transferring free electrons than metal oxides for $BaTi_4O_9$ in photocatalytic reactions from aqueous ethanol solution. Afterwards, the modification of Pt loading was focused to investigate the influence of calcination temperature on photocatalytic activities.

The photocatalytic activity of Pt/$BaTi_4O_9$ as a function of calcination temperature is shown in Fig. 7. In photocatalytic H_2 evolution from pure water, the activity achieved a maximum at 700 °C with an evolution rate of 65 μmol h^{-1}, indicating its relatively large surface area contributes a lot in providing substantial active sites for photocatalytic water decomposition. When 20 ml ethanol was introduced, a remarkable increase of photoactivity can be clearly observed. The activity passed through an optimum level of 855 μmol h^{-1} at 800 °C, and decreased sharply with raising temperatures. The highest value of apparent quantum yield for H_2 evolution from pure water and aqueous ethanol solution was 0.9% and 11.7% apart, respectively obtained over 0.1 g Pt/$BaTi_4O_9$ calcined at 700 and 800 °C by the PC method. The SSR sample calcined at 1,100 °C only showed a photocatalytic activity of 174 μmol h^{-1}, which was mainly caused by its low surface area together with the imperfect crystallization. A correlation that the tunnel structure titanate with a high ability of

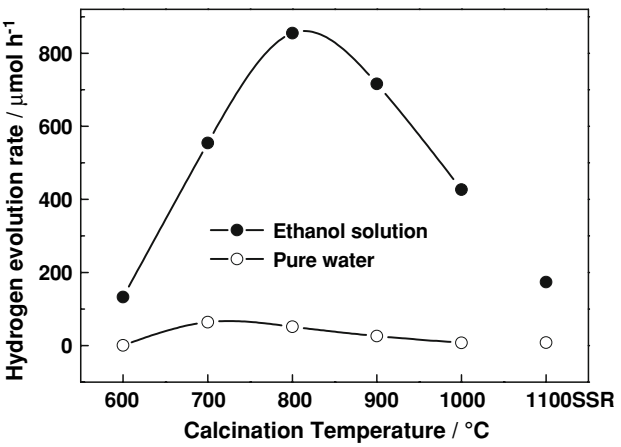

Fig. 7 The effect of calcination temperature on the photocatalytic H_2 evolution from pure water and ethanol solution over Pt/$BaTi_4O_9$ synthesized by the PC and SSR method

O^- radical formation under UV irradiation favors photocatalytic reaction has been demonstrated [25, 26]. The O^- surface species is proposed to be responsible for holes center, and meantime the Ti^{3+} species would help promote the reduction of H^+ by transferring the photoexcited electrons to Pt particles [26]. The cyclic process of bond scission and re-bonding between the Ti and O ions is essential in photoreactions of $BaTi_4O_9$. Therefore, the best photocatalytic activity obtained over Pt/$BaTi_4O_9$ at 800 °C does not only account for a good balance between enough surface area and improved crystallinity, but also has intimate relationships with the active species of Ti^{3+} and O^-. As discussed above, the relatively high PL intensity of $BaTi_4O_9$ calcined at 800 °C may suggest the increased content of Ti^{3+} *d*-orbital surface states stabilized by oxygen vacancy in the forbidden gap. It implies that adequate amounts of Ti^{3+} and O^- radicals would be provided in photoreactions as electron carriers to Pt particles and hole centers for oxidation of ethanol separately, leading to the decreased possibility of photogenerated electron-hole recombinations and great enhancement in the photocatalytic activity of H_2 evolution.

4 Conclusions

$BaTi_4O_9$ powder has been successfully synthesized by the PC method at reduced temperatures (700–1,000 °C) for a shorter calcination time relative to the SSR method. Although some unstoichiometric impurity phases were detected in XRD patterns, the PC-derived $BaTi_4O_9$ has prominent advantage in improved crystal homogeneity and relatively large surface area compared to the SSR sample. Among different loading cocatalysts investigated, NiO_x– and RuO_x–$BaTi_4O_9$ can split water into H_2 and O_2 in a nearly stoichiometric ratio, but no promotion of photoreactions occurred when ethanol was introduced as holes scavenger. In this study, Pt/$BaTi_4O_9$ was identified as the most efficient photocatalyst toward photocatalytic H_2 evolution from aqueous ethanol solution. The maximum photocatalytic activity was achieved over Pt loaded $BaTi_4O_9$ calcined at 800 °C by the PC method. It was not only attributed to an appropriate balance between large surface area and improved crystallinity, but also to its ability to provide considerable lattice O^- and Ti^{3+} radicals to prevent electron-hole recombinations.

Acknowledgments The work was financially supported by the National Basic Research Program of China (973 Program) (No. 2003CB214500), National HighTechnology Research and Development Program of China (863 Program) (No. 2006AA03Z223), Specialized Research Fund for the Doctoral Program of Higher Education of China (No. 20030003069) and "Solar Hydrogen" Project sponsored by Shell Hydrogen.

References

1. Ikeda S, Hara M, Kondo JN, Domen K, Takahashi H, Okubo T, Kakihana M (1998) Chem Mater 10:72
2. Ogura S, Sato K, Inoue Y (2000) Phys Chem Chem Phys 2:2449
3. Ko YG, Lee WY (2002) Catal Lett 83:157
4. Hwang DW, Kirn HG, Lee JS, Kim J, Li W, Oh SH (2005) J Phys Chem B 109:2093
5. Sun W, Zhang S, Wang C, Liu ZX, Mao ZQ (2007) Catal Lett 119:148
6. Inoue Y, Asai Y, Sato K (1994) J Chem Soc Faraday Trans 90:797
7. Kakihana M, Arima M, Sato T, Yoshida K, Yamashita Y, Yashima M, Yoshimura M (1996) Appl Phys Lett 69:2053
8. Yamashita Y, Yoshida K, Kakihana M, Uchida S, Sato T (1999) Chem Mater 11:61
9. Yamashita Y, Tada M, Kakihana M, Osada M, Yoshida K (2002) J Mater Chem 12:1782
10. Kohno M, Kaneko T, Ogura S, Sato K, Inoue Y (1998) J Chem Soc Faraday Trans 94:89
11. Inoue Y, Niiyama T, Asai Y, Sato K (1992) J Chem Soc Chem Commun 579
12. Sato J, Kobayashi H, Inoue Y (2003) J Phys Chem B 107:7970
13. Yoshino M, Kakihana M (2002) Chem Mater 14:3369
14. Abe R, Higashi M, Sayama K, Abe Y, Sugihara H (2006) J Phys Chem B 110:2219
15. Hwang DW, Kim HG, Kim J, Cha KY, Kim YG, Lee JS (2000) J Catal 193:40
16. Xu YB, Yuan X, Lu PX, Huang GH (2006) Mater Chem Phys 96:427
17. Hirano M, Nakahara C, Ota K, Tanaike O, Inagaki M (2003) J Solid State Chem 170:39
18. Pontes FM, Pinheiro CD, Longo E, Leite ER, de Lazaro SR, Varela JA, Pizani PS, Boschi TM, Lanciotti F (2003) Mater Chem Phys 78:227
19. Yamashita H, Ichihashi Y, Zhang SG, Matsumura Y, Souma Y, Tatsumi T, Anpo M (1997) Appl Surf Sci 121:305
20. Rahman MM, Krishna KM, Soga T, Jimbo T, Umeno M (1999) J Phys Chem Solids 60:201
21. Meng JF, Huang YB, Zhang WF, Du ZL, Zhu ZQ, Zou GT (1995) Phys Lett A 205:72
22. Li XZ, Li FB, Yang CL, Ge WK (2001) J Photochem Photobiol A 141:209
23. Yin J, Zou ZG, Ye JH (2003) J Phys Chem B 107:61
24. Patsoura A, Kondarides DI, Verykios XE (2006) J Appl Catal B Environ 64:171
25. Kohno M, Ogura S, Sato K, Inoue Y (1997) Chem Phys Lett 267:72
26. Kohno M, Ogura S, Sato K, Inoue Y (1997) J Chem Soc Faraday Trans 93:2433